

MACU-Net: Semantic Segmentation from High-Resolution Remote Sensing Images

Rui Li*, Chenxi Duan*, and Shunyi Zheng

Abstract—Semantic segmentation of remote sensing images plays an important role in land resource management, yield estimation, and economic assessment. U-Net is a sophisticated encoder-decoder architecture which has been frequently used in medical image segmentation and has attained prominent performance. And asymmetric convolution block can enhance the square convolution kernels using asymmetric convolutions. In this paper, based on U-Net and asymmetric convolution block, we incorporate multi-scale features generated by different layers of U-Net and design a multi-scale skip connected architecture, MACU-Net, for semantic segmentation using high-resolution remote sensing images. Our design has the following advantages: (1) The multi-scale skip connections combine and realign semantic features contained both in low-level and high-level feature maps with different scales; (2) the asymmetric convolution block strengthens the representational capacity of a standard convolution layer. Experiments conducted on two remote sensing image datasets captured by separate satellites demonstrate that the performance of our MACU-Net transcends the U-Net, SegNet, DeepLab V3+, and other baseline algorithms.

Index Terms—high-resolution remote sensing images, asymmetric convolution block, semantic segmentation

I. INTRODUCTION

Semantic segmentation using remote sensing images, i.e., the assignment of assigning the precise category to every pixel contained in an image [1, 2], plays a critical role in wide range of application scenarios such as land resource management, yield estimation, and economic assessment [3-5]. Hitherto the remote sensing community has tried to design assorted classifiers from diverse perspectives, from orthodox methods such as distance measure [6], to advanced methods including support vector machine (SVM) [7] and random forest (RF) [8]. However, the high dependency on hand-crafted visual features or mid-level semantic features restricts the flexibility and adaptability of these methods.

More recently, Convolutional Neural Networks (CNN) [9] have demonstrated its powerful capacity of automatically capture nonlinear and hierarchical features from images, and have dramatically influenced the field of computer vision (CV) [10]. For semantic segmentation, the encoder-decoder frameworks such as SegNet [11], U-Net [12], and DeepLab [13, 14] have become the frequently-used schemes. Generally,

feature maps generated by the encoder comprise low-level and fine-grained detailed information, while feature maps generated by the decoder contain high-level and coarse-gained semantic information [15]. And skip connections, which combine the low-level and high-level feature maps, are an effective method to boost the semantic extraction ability of encoder-decoder frameworks.

In U-Net++ [15], plain skip connections are substituted by nested and dense skip connections, which enhance the ability of skip connections and narrow the semantic gap between the encoder and decoder. To make utmost of the multi-scale features, the full-scale skip connections are designed in U-Net 3+ [16]. However, the design philosophy of full-scale skip connections impliedly indicates that all channels of feature maps generated by different layers share equal weights, and the computational complexity of U-Net 3+ is tremendous. On the contrary, the features generated by different stages own different levels of discrimination. To cope with this issue, in our MACU-Net, we propose a multi-scale skip connection which not only takes full advantages of the multi-scale features, but also realigns channel-wise features responses adaptively.

Asymmetric convolution blocks (ACB), which own branches with square, horizontal and vertical kernels, could capture refined features by summing up the outputs of three convolutions, which just cause finite increasing in additional computational complexity [17]. The effectiveness of ACB has been verified in the fields including image classification [17], image denoising [18], and medical image segmentation [19]. In [19], only the convolutional layers of encoder are replaced by ACB. Aiming at the task of high-resolution remote sensing image segmentation, we thoroughly incorporate ACB with U-Net by substitute all convolutional layers to enhance the representational ability of a standard square-kernel layer.

Based on the above-mentioned insight and progress, we design a multi-scale connected architecture deep network, MACU-Net with asymmetric convolution blocks. To verify the effectiveness of MACU-Net, we compare the performance of proposed algorithm with SegNet [11], U-Net [12], DeepLab V3 [13], DeepLab V3+ [14], FC-DenseNet57 [20], Attention U-Net [21], FGC [22], MSFCN, and U-Net++ [15]. The major

*These authors contributed equally to this work.

This work was supported in part by the National Natural Science Foundations of China (No. 41671452). (Corresponding author: Rui Li.)

R. Li and S. Zheng are with School of Remote Sensing and Information Engineering, Wuhan University, Wuhan 430079, China (e-mail: ironui@whu.edu.cn; syzheng@whu.edu.cn).

C. Duan is with the State Key Laboratory of Information Engineering in Surveying, Mapping, and Remote Sensing, Wuhan University, Wuhan 430079, China; chenxiduan@whu.edu.cn (e-mail: chenxiduan@whu.edu.cn).

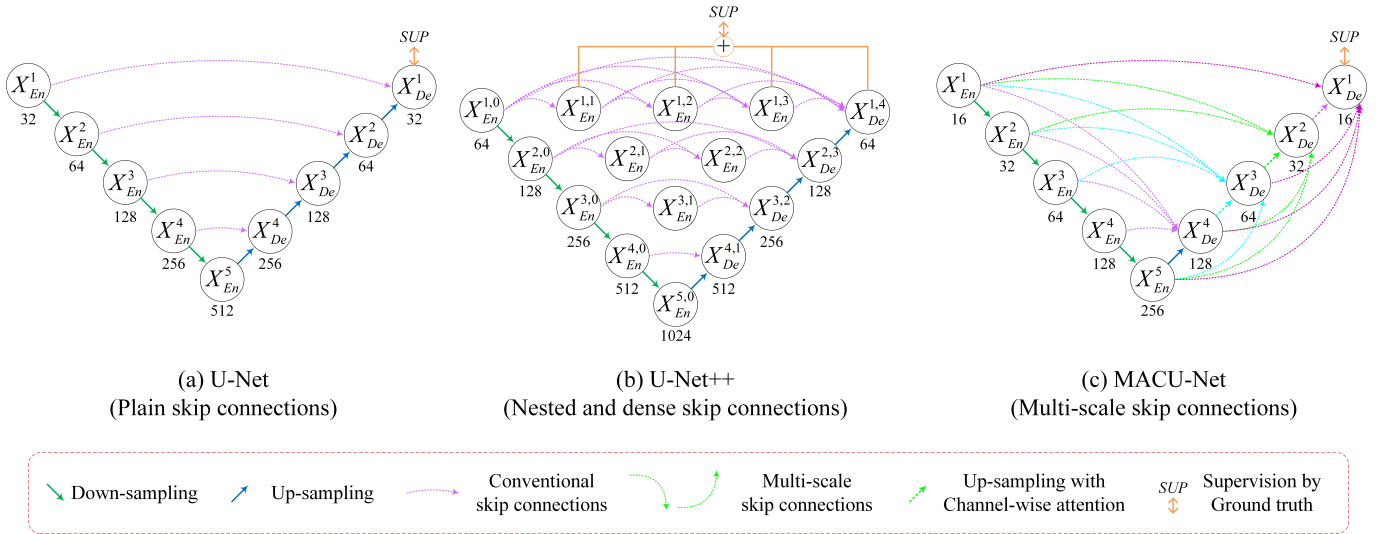


Fig. 1. Comparison of (a) U-Net, (b) U-Net++, and proposed (c) MACU-Net 3+. The depth of each node is presented below the circle.

contributions of this letter could be listed as follows:

- 1) To take full advantages of the multi-scale features, we design a multi-scale skip connection which can realign channel-wise features responses adaptively.
- 2) We substitute all convolutional layers of U-Net for asymmetric convolution blocks substitute to enhance the representational ability.
- 3) Based on multi-scale skip connections and asymmetric convolution blocks, we proposed MACU-Net, and a series of experiments demonstrate the effectiveness of proposed algorithm.

The remainder of this letter is arranged as follows: In Section 2, we illustrate the detailed structure of proposed MACU-Net. The experimental results are provided and analyzed in Sections 3. Finally, in Section 4 we draw a conclusion of the whole letter.

II. METHODOLOGY

Fig.1 gives graphical overviews of U-Net, U-Net++ and the proposed MACU-Net. Compared with U-Net and U-Net++, the multi-scale features of MACU-Net are combined by re-designing skip connections.

A. Asymmetric Convolution Block

Objects may be captured by satellites in any possible orientations. Thus, objects in remote sensing images may be presented at any perspective, which can be summarized as rotation. In order to extract available information contained in remote sensing images, the neural network should be robust to rotation and renders consistent results in different rotations. As reported in [17], different asymmetric convolutions are robust with different rotation objects. As can be seen from Fig.2, 3×1 kernel is insensitive to horizontal flipping. Hence, asymmetric convolutions are viable schemes to boost the rotation robustness of the neural network.

Based on above-mentioned insight, we modify the asymmetric convolutions proposed in [17] and design an asymmetric convolution block (ACB) to capture features from different receptive fields, which can be seen from Fig.3. There are three branches in ACB, i.e. 3×3 convolution, a 1×3 convolution, and a 3×1 convolution, to get different information.

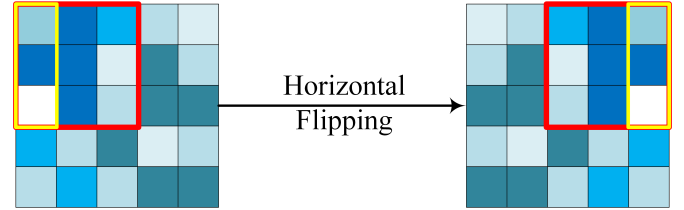


Fig. 2. Comparison between 3×3 kernel (red) and 3×1 kernel (yellow). The 3×1 kernel obtains the same results on horizontal flipped input, but 3×3 kernel attains different result.

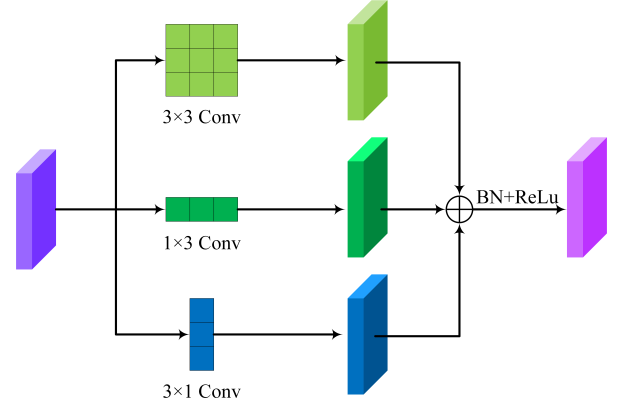


Fig. 3. The structure of asymmetric convolution block.

The 3×3 convolution captures features by a relatively large receptive field, while the 1×3 and 3×1 convolutions curb the rotation sensibility of vertical and horizontal flipping separately. Meanwhile, ACB expand the width of the network. The feature maps generated by three branches are added up to obtain fusion result. Finally, batch norm (BN) and ReLU are used to boost the numerical stability and activate the result in a nonlinear manner. The formulation of ACB can be described as:

$$\bar{x}_i = F_{3 \times 3}(x_{i-1}) + F_{1 \times 3}(x_{i-1}) + F_{3 \times 1}(x_{i-1}) \quad (1)$$

$$x_i = \sigma \left(\gamma_i \frac{\bar{x}_i - E(\bar{x}_i)}{\sqrt{Var(\bar{x}_i)} + \epsilon_i} + \beta_i \right) \quad (2)$$

where x_i is the output of the ACB, and x_{i-1} is the input of the ACB. $Var(\cdot)$ and $E(\cdot)$ represent the variance function and

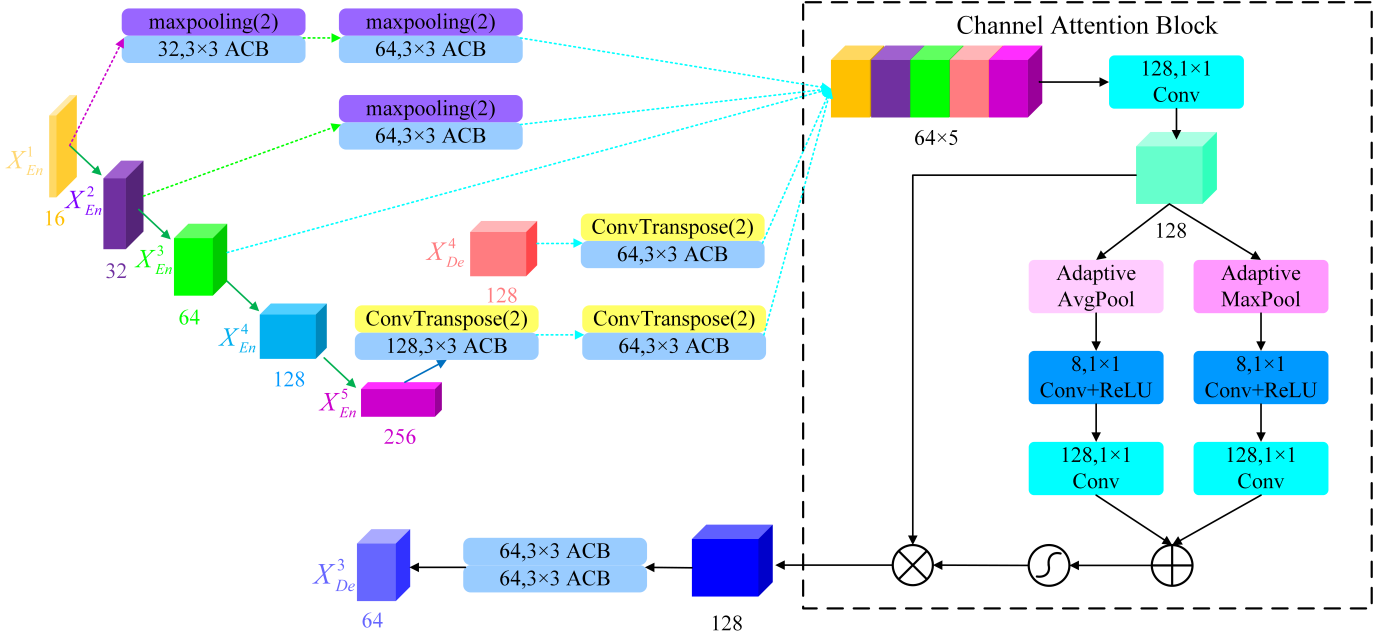


Fig. 4. Illustration of how to construct the multi-scale aggregated feature map of X_{De}^3 .

expectation of the input. ϵ is a small constant to maintain numerical stability. γ and β are two trainable parameters of BN layer, and the normalized result can be scaled by γ and shifted by β . $\sigma(\cdot)$ denotes the activation function ReLU.

ACB is used to capture and refine the features of objects in each layer of the encoder, and is attached after each transposed convolution of decoder to avoid the checkerboard pattern and generate smooth image.

B. Multi-Scale Skip Connections

As information from multi-scales are not fully exploit both by plain connections of U-Net and nested and dense connections of U-Net++, we design the multi-scale skip connections to capture the interplay between the encoder and decode and extract both fine-grained detailed information and coarse-grained semantic information.

Taking X_{De}^3 as an example, Fig. 4 demonstrates how to generated the feature maps. Firstly, the feature maps of the same-level encoder layer, i.e. X_{En}^3 , are directly connected. Secondly, the fine-grained detailed information contained in lower-level encoder layers, i.e. X_{De}^4 and X_{De}^5 , are delivered by transposed convolution and asymmetric convolution block. Thirdly, the coarse-grained semantic information contained in higher-level encoder layers, i.e. X_{En}^1 and X_{En}^2 , are transmitted by max-pooling and asymmetric convolution block. The above procedure can be formulated as:

$$X_{De}^i = \begin{cases} X_{En}^i, i = N \\ CAB \left(\begin{bmatrix} A(D(X_{En}^k)_{k=1}^{i-1}), A(U(X_{De}^k)_{k=i+1}^N) \\ Scales: 1^{th} \sim i^{th} & Scales: (i+1)^{th} \sim N^{th} \end{bmatrix} \right), \\ i = 1, \dots, N-1 \end{cases} \quad (3)$$

where CAB indicates channel attention block which realigns channel-wise features, and $A(\cdot)$ denotes asymmetric convolution block. $D(\cdot)$ and $U(\cdot)$ represent down-sampling using max-pooling layer and up-sampling using transposed

convolution respectively, and $[\cdot]$ represents the operation of concatenation.

C. Channel Attention Block

With five feature maps with identical size and resolution in hand, we need to further decrease the prodigious number of channels, as well as realign channel-wise features. Motivated by Convolutional Block Attention Module (CBAM) [23], we design the channel attention block (CAB) to reweighting the channel-wise features, which can be seen from the right of Fig.4. The aim of CAB is to learn a 1-D weight $W_c \in R^{C \times 1 \times 1}$ which weights the channels of input feature map $F \in R^{C \times H \times W}$, where C , W , and H indicate the number of channels, the height, and the width of the feature map. By multiplying W_c and F , CAB enhances the discriminative channels and restrains the indiscriminative channels.

First of all, we use a 1×1 convolution with 128 filters to reduce the number of channels. Then, the spatial dimension is squeezed by the operation of an average-pooling and a max-pooling simultaneously. By two convolution layers with 8 filters and ReLU activation functions, the channels of squeezed feature maps are compressed to one-sixteenth of its original number, and then channels are reinstated using two convolution layers with 128 filters. Finally, the sum of two layers is activated by sigmoid and then multiply by the output of the first convolution.

III. EXPERIMENTAL RESULTS

This section first introduces the datasets and experimental settings to verify the effectiveness of MACU-Net, and then compares the performance between different frameworks.

A. Datasets

The effectiveness of MACU-Net is verified using Wuhan Dense Labeling Dataset (WHDL) [24, 25] and Gaofen Image Dataset (GID) [30].

WHDL D contains 4940 RGB images in the size of 256×256 captured by Gaofen 1 Satellite and ZY-3 Satellite over Wuhan urban area. By image fusion and resampling, the images resolution is reach to 2m/pixel. The images contained in WHDL D are labeled with six classes, i.e. bare soil, building, pavement, vegetation, road, and water.

GID contains 150 RGB images in the size of 7200×6800 captured by Gaofen 2 Satellite over 60 cities in China. Each image covering a geographic region of 506 km^2 . The images contained in GID are labeled with six classes, i.e. build-up, forest, farmland, meadow, water, and others. We just select 15 images contained in GID. The principle of selection is to cover whole six classes. And the serial number of the selected images will be released with our open source code ¹

B. Experimental Setting

To evaluate the effectiveness of MACU-Net, SegNet [11], U-Net [12], DeepLab V3 [13], DeepLab V3+ [14], FC-DenseNet57 (tiramisu) [20], Attention U-Net [21], FGC [22], MSFCN, and U-Net++ [15]. Excluding SegNet, DeepLab V3 and DeepLab V3+, the remaining methods are all improved version of U-Net.

All of the models are implemented with PyTorch, and the optimizer is set as Adam with 0.0001 learning rate and 16 batch size. All the experiments are implemented on a single NVIDIA GeForce RTX 2080ti GPU with 11 GB RAM. The cross-entropy loss function is used as quantitative evaluation and backpropagation index to measure the disparity between the obtained 2D segmentation maps and ground truth.

For WHDL D, we randomly select 60% images as training set, 20% images as validation set, and the rest 20% images as test set. For GID, we separately partition each image into non-overlap patch sets with the size of 256×256 , and just discard the pixels on the edges which cannot be divisible by 256. Thus, 10920 patches are obtained. Then we randomly select 60% patches as training set, 20% patches as validation set, and the rest 20% patches as test set.

For each dataset, the overall accuracy (OA), average accuracy (AA), Kappa coefficient (K), mean Intersection over Union (mIoU), Frequency Weighted Intersection over Union (FWIoU), and F1-score (F1) are adopted as evaluation indexes.

C. Results on WHDL D and GID

The experimental results of different methods on WHDL D and GID are demonstrated in Table I and Table II. The performance of proposed MAC-UNet transcends other algorithms in all quantitative evaluation indexes, which can be seen from tables. For WHDL D, the proposed MACU-Net brings near 0.8% improvements on mIoU compared with U-Net++. And for GID dataset, the improvements are more than 1.4% in mIoU and nearly 1% in F1-score, respectively. Some visual results generated by our method and U-Net are provided in Fig. 5 and Fig. 6, which manifest that the proposed MACU-Net can capture refined features.

What is more, the number of parameters and the consumptions of calculation are also significant to assess the merit of a framework. The comparison of parameters and

TABLE I
THE EXPERIMENTAL RESULTS ON WHDL D DATASET.

Method	OA	AA	K	mIoU	FWIoU	F1
SegNet	80.229	63.787	71.403	52.940	68.876	66.529
DeepLab V3	79.611	67.515	71.001	54.992	68.409	68.804
U-Net	82.864	68.730	75.736	57.410	73.449	70.278
Tiramisu	82.188	70.712	74.903	58.167	72.243	71.276
U-NetAtt	82.602	69.738	75.484	56.918	73.474	69.622
FGC	82.975	68.855	75.927	57.368	73.540	70.274
MSFCN	<u>84.168</u>	72.081	<u>77.558</u>	60.366	<u>74.892</u>	73.031
DeepLab V3+	83.568	73.053	76.740	61.194	73.894	74.047
U-Net++	84.067	<u>74.004</u>	77.430	<u>61.799</u>	74.496	<u>74.633</u>
MACU-Net	84.623	74.568	78.233	62.600	75.231	75.245

TABLE II
THE EXPERIMENTAL RESULTS ON GID DATASET.

Method	OA	AA	K	mIoU	FWIoU	F1
SegNet	80.035	82.396	74.612	70.962	67.420	82.290
DeepLab V3	80.072	83.182	74.741	71.348	67.632	82.672
U-Net	79.754	81.677	74.219	70.535	67.129	82.113
Tiramisu	79.467	84.808	74.377	69.032	65.627	80.716
U-NetAtt	80.919	83.838	75.878	70.930	68.539	82.511
FGC	81.180	84.716	76.270	72.067	68.859	83.240
MSFCN	82.520	85.042	77.897	73.637	71.047	85.378
DeepLab V3+	82.667	<u>85.065</u>	78.012	<u>74.109</u>	71.409	84.678
U-Net++	<u>83.221</u>	84.942	<u>78.723</u>	74.105	<u>71.973</u>	84.725
MACU-Net	84.062	86.136	79.819	75.587	73.290	85.700

computational complexity between different algorithms are reported in Table III, where ‘M’ is the abbreviation of million, the unit of parameter number, and ‘G’ is the abbreviation of Gillion (thousand million), the unit of floating point operations. And the comparison demonstrates that the design of MACU-Net is efficient.

TABLE III
THE COMPARISON OF PARAMETERS AND COMPUTATIONAL COMPLEXITY.

Method	input shape	Parameters (M)	Complexity (G)
SegNet		29.45	40.29
DeepLab V3		58.16	18.63
U-Net		10.86	13.94
Tiramisu		1.38	11.92
U-NetAtt		2.17	12.75
FGC	$3 \times 256 \times 256$	2.19	8.4
MSFCN		2.67	9.66
DeepLab V3+		59.46	23.98
UNet++		9.05	29.94
MACU-Net		5.28	7.43

IV. CONCLUSION

In this letter, to implement semantic segmentation of high-resolution remote sensing images, we combine multi-scale features generated by different layers of U-Net and design a multi-scale skip connected architecture, MACU-Net. Using multi-scale skip connections and channel attention blocks, semantic features generated by different layers of U-Net are combined and refined. Meanwhile, the representational capacity of the standard convolution layer is enhanced by the asymmetric convolution block. Experiments conducted on two large-scale datasets manifest the performance of our MACU-Net transcends nine baseline algorithms.

¹ <https://github.com/lironui/U-Net-with-Multi-Scale-Skip-Connections-and-Asymmetric-Convolution-Blocks>.

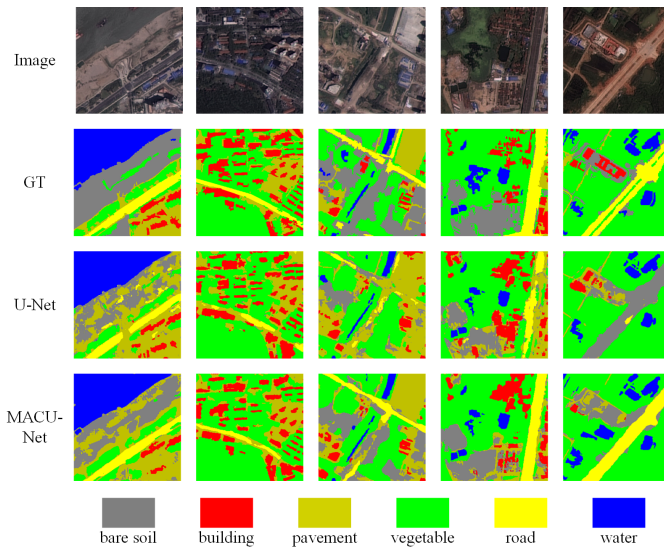


Fig. 5. Visualization of results on WHDL.

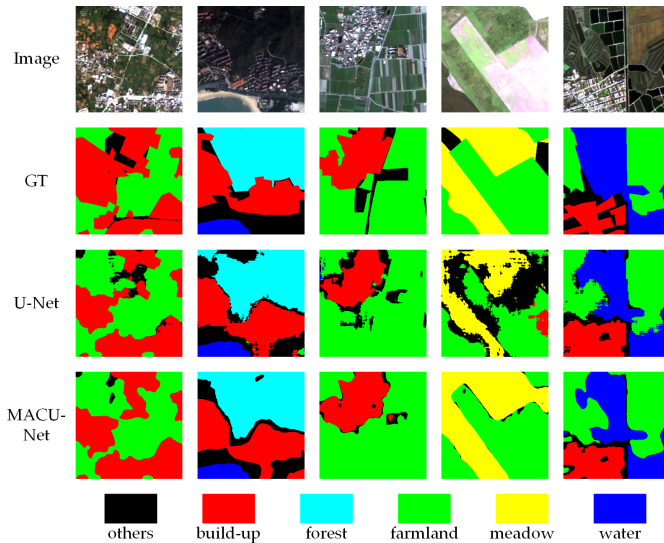


Fig. 6. Visualization of results on GID.

REFERENCES

- [1] J. Long, E. Shelhamer, and T. Darrell, "Fully convolutional networks for semantic segmentation," in *Proceedings of the IEEE conference on computer vision and pattern recognition*, 2015, pp. 3431-3440.
- [2] D. Marmanis, J. D. Wegner, S. Galliani, K. Schindler, M. Datcu, and U. Stilla, "Semantic segmentation of aerial images with an ensemble of CNSS," *ISPRS Annals of the Photogrammetry, Remote Sensing and Spatial Information Sciences*, 2016, vol. 3, pp. 473-480, 2016.
- [3] J. Zhang, L. Feng, and F. Yao, "Improved maize cultivated area estimation over a large scale combining MODIS-EVI time series data and crop phenological information," *ISPRS journal of photogrammetry and remote sensing*, vol. 94, pp. 102-113, 2014.
- [4] C. Zhang *et al.*, "Joint Deep Learning for land cover and land use classification," *Remote sensing of environment*, vol. 221, pp. 173-187, 2019.
- [5] D. Sulla-Menashe, J. M. Gray, S. P. Abercrombie, and M. A. Friedl, "Hierarchical mapping of annual global land cover 2001 to present: The MODIS Collection 6 Land Cover product," *Remote sensing of environment*, vol. 222, pp. 183-194, 2019.
- [6] N. Li, H. Huo, and T. Fang, "A novel texture-preceded segmentation algorithm for high-resolution imagery," *IEEE Transactions on Geoscience and Remote Sensing*, vol. 48, no. 7, pp. 2818-2828, 2010.
- [7] X. Huang and L. Zhang, "An SVM ensemble approach combining spectral, structural, and semantic features for the classification of high-resolution remotely sensed imagery," *IEEE Transactions on Geoscience and Remote Sensing*, vol. 51, no. 1, pp. 257-272, 2012.
- [8] S. Du, F. Zhang, and X. Zhang, "Semantic classification of urban buildings combining VHR image and GIS data: An improved random forest approach," *ISPRS journal of photogrammetry and remote sensing*, vol. 105, pp. 107-119, 2015.
- [9] A. Krizhevsky, I. Sutskever, and G. E. Hinton, "Imagenet classification with deep convolutional neural networks," in *Advances in neural information processing systems*, 2012, pp. 1097-1105.
- [10] Z. Liu, P. Luo, X. Wang, and X. Tang, "Deep learning face attributes in the wild," in *Proceedings of the IEEE international conference on computer vision*, 2015, pp. 3730-3738.
- [11] V. Badrinarayanan, A. Kendall, and R. Cipolla, "Segnet: A deep convolutional encoder-decoder architecture for image segmentation," *IEEE transactions on pattern analysis and machine intelligence*, vol. 39, no. 12, pp. 2481-2495, 2017.
- [12] O. Ronneberger, P. Fischer, and T. Brox, "U-net: Convolutional networks for biomedical image segmentation," in *International Conference on Medical image computing and computer-assisted intervention*, 2015: Springer, pp. 234-241.
- [13] L.-C. Chen, G. Papandreou, F. Schroff, and H. Adam, "Rethinking atrous convolution for semantic image segmentation," *arXiv preprint arXiv:1706.05587*, 2017.
- [14] L.-C. Chen, Y. Zhu, G. Papandreou, F. Schroff, and H. Adam, "Encoder-decoder with atrous separable convolution for semantic image segmentation," in *Proceedings of the European conference on computer vision (ECCV)*, 2018, pp. 801-818.
- [15] Z. Zhou, M. M. R. Siddiquee, N. Tajbakhsh, and J. Liang, "Unet++: A nested u-net architecture for medical image segmentation," in *Deep Learning in Medical Image Analysis and Multimodal Learning for Clinical Decision Support*: Springer, 2018, pp. 3-11.
- [16] H. Huang *et al.*, "UNet 3+: A Full-Scale Connected UNet for Medical Image Segmentation," in *ICASSP 2020-2020 IEEE International Conference on Acoustics, Speech and Signal Processing (ICASSP)*, 2020: IEEE, pp. 1055-1059.
- [17] X. Ding, Y. Guo, G. Ding, and J. Han, "Acnet: Strengthening the kernel skeletons for powerful cnn via asymmetric convolution blocks," in *Proceedings of the IEEE International Conference on Computer Vision*, 2019, pp. 1911-1920.
- [18] A. Abdelhamed, M. Afifi, R. Timofte, and M. S. Brown, "Ntire 2020 challenge on real image denoising: Dataset, methods and results," in *Proceedings of the IEEE/CVF Conference on Computer Vision and Pattern Recognition Workshops*, 2020, pp. 496-497.
- [19] Y. Cheng, Y. Gao, L. Xie, X. Xie, and W. Lin, "Spatial Enhanced Rotation Aware Network for Breast Mass Segmentation in Digital Mammogram," *IEEE Access*, 2020.
- [20] S. Jégou, M. Drozdal, D. Vazquez, A. Romero, and Y. Bengio, "The one hundred layers tiramisú: Fully convolutional densenets for semantic segmentation," in *Proceedings of the IEEE conference on computer vision and pattern recognition workshops*, 2017, pp. 11-19.
- [21] O. Oktay *et al.*, "Attention u-net: Learning where to look for the pancreas," *arXiv preprint arXiv:1804.03999*, 2018.
- [22] S. Ji, Z. Zhang, C. Zhang, S. Wei, M. Lu, and Y. Duan, "Learning discriminative spatiotemporal features for precise crop classification from multi-temporal satellite images," *International Journal of Remote Sensing*, vol. 41, no. 8, pp. 3162-3174, 2020.
- [23] S. Woo, J. Park, J.-Y. Lee, and I. So Kweon, "Cbam: Convolutional block attention module," in *Proceedings of the European conference on computer vision (ECCV)*, 2018, pp. 3-19.
- [24] Z. Shao, K. Yang, and W. Zhou, "Performance evaluation of single-label and multi-label remote sensing image retrieval using a dense labeling dataset," *Remote Sens.*, vol. 10, no. 6, p. 964, 2018.
- [25] Z. Shao, W. Zhou, X. Deng, M. Zhang, and Q. Cheng, "Multilabel Remote Sensing Image Retrieval Based on Fully Convolutional Network," *IEEE J. Sel. Top. Appl. Earth Obs. Remote Sens.*, vol. 13, pp. 318-328, 2020.